

# Lattice study on $\pi K$ scattering with moving wall source

Ziwen Fu

*Key Laboratory of Radiation Physics and Technology (Sichuan University), Ministry of Education; Institute of Nuclear Science and Technology, Sichuan University, Chengdu 610064, P. R. China.*

The  $s$ -wave pion-kaon ( $\pi K$ ) scattering lengths at zero momentum are calculated in lattice QCD with sufficiently light  $u/d$  quarks and strange quark at its physical value by the finite size formula. The light quark masses correspond to  $m_\pi = 0.330 - 0.466$  GeV. In the “Asqtad” improved staggered fermion formulation, we measure the  $\pi K$  four-point correlators for both isospin  $I = 1/2$  and  $3/2$  channels, and analyze the lattice simulation data at the next-to-leading order in the continuum three-flavor chiral perturbation theory, which enables us a simultaneous extrapolation of  $\pi K$  scattering lengths at physical point. We adopt a technique with the moving wall sources without gauge fixing to obtain the substantiable accuracy, moreover, for  $I = 1/2$  channel, we employ the variational method to isolate the contamination from the excited states. Extrapolating to the physical point yields the scattering lengths as  $m_\pi a_{3/2} = -0.0505(19)$  and  $m_\pi a_{1/2} = 0.1827(37)$  for  $I = 3/2$  and  $1/2$  channels, respectively. Our simulation results for  $\pi K$  scattering lengths are in agreement with the experimental reports and theoretical predictions, and can be comparable with other lattice simulations. These simulations are carried out with MILC  $N_f = 2 + 1$  flavor gauge configurations at lattice spacing  $a \approx 0.15$  fm.

PACS numbers: 12.38.Gc

## I. INTRODUCTION

Pion-kaon ( $\pi K$ ) scattering at low energies is the simplest reactions including a strange quark, and it allows for an explicit exploration of the three-flavor structure of the low-energy hadronic interactions, which is not directly probed in the  $\pi\pi$  scattering. The measurement of  $\pi K$  scattering lengths is one of the cleanest processes and a decisive test for our understanding of the chiral SU(3) symmetry breaking of the quantum chromodynamics (QCD). In the present study, we will concentrate on the  $s$ -wave scattering lengths of  $\pi K$  system, which have two isospin eigenchannels ( $I = 3/2, 1/2$ ) in the isospin limit, and the low-energy interaction is repulsive for  $I = 3/2$  channel, and attractive for  $I = 1/2$  case, respectively.

Experimentally,  $\pi K$  scattering lengths are obtained through  $\pi K$  scattering phases using the Roy-Stainer equations. The experiments at low energies are an important method in the study of the interactions among mesons [1–3], and these experiments have reported that the  $s$ -wave scattering length ( $a_0$ ) in the  $I = 3/2$  channel,  $m_\pi a_{3/2}$  has a small negative value, namely,  $-0.13 \sim -0.05$ . Moreover, the on-going experiments proposed by the DIRAC collaboration [4] to examine  $\pi K$  atoms will provide the direct measurements or constraints on  $\pi K$  scattering lengths.

At present, theory predicts  $\pi K$  scattering lengths with a precision of about 10%, and it will be significantly improved in the near future. Through the scalar form factors in semi-leptonic pseudo-scalar-to-pseudo-scalar decays, Flynn et al. [5] extracted the  $\pi K$  scattering length in the  $I = 1/2$  channel as  $m_\pi a_{1/2} = +0.179(17)(14)$ . Three-flavor Chiral Perturbation Theory ( $\chi$ PT) [6–9] has been used to predict the scattering lengths in the study of the low-energy  $\pi K$  scattering, and small negative value

was claimed as  $m_\pi a_{3/2} = -0.129 \sim -0.05$ . However, if the scattering hadrons contain strange quarks,  $\chi$ PT predictions usually suffer from considerable corrections due to the chiral SU(3) flavor symmetry breaking, as compared with the case of the  $\pi\pi$  scattering. Therefore, a lattice QCD calculation is needed to offer an alternative important consistent check of the validity of  $\chi$ PT in the presence of the strange quarks.

To date, four lattice studies of  $\pi K$  scattering length have been reported [10–13]. The first lattice calculation of  $\pi K$  scattering length in  $I = 3/2$  channel was explored by Miao et al. [10] using the quenched approximation, and the value of  $m_\pi a_{3/2}$  was found to be  $-0.048$ . The first fully-dynamical calculation using  $N_f = 2 + 1$  flavors of the Asqtad-improved [14, 15] staggered sea quark [16, 17] was carried out [11] to calculate the  $I = 3/2$  scattering length for  $m_\pi = 0.29 - 0.60$  GeV, and further indirectly evaluate the  $I = 1/2$  scattering length on the basis of  $\chi$ PT. They obtained a small negative value of  $m_\pi a_{3/2} = -0.0574$  for  $I = 3/2$  channel and a positive value of  $m_\pi a_{1/2} = 0.1725$  for  $I = 1/2$  channel, respectively. Nagata et al. fulfilled first direct lattice calculation on  $I = 1/2$  channel [12] using the quenched approximation. They investigated all quark diagrams contributing to both isospin eigenstates, and found that the scattering amplitudes can be expressed as the combinations of only three diagrams in the isospin limit. This work greatly inspires us to study  $\pi K$  scattering. However, they did not observe the repulsive interaction even for  $I = 3/2$  channel at their simulation points, and their lattice calculations are relatively cheaper. Sasaki et al. observed the correct repulsive interaction for  $I = 3/2$  channel and attractive for  $I = 1/2$  case, and they obtained the scattering lengths of  $m_\pi a_{3/2} = -0.0500(68)$  and  $m_\pi a_{1/2} = 0.154(28)$  for the  $I = 3/2$  and  $1/2$  channels, respectively [13]. Moreover, to isolate the contam-

ination from the excited states, they construct a  $2 \times 2$  matrix of the time correlation function and diagonalize it [13], this method will guide us to study  $\pi K$  scattering for  $I = 1/2$  channel in a correct manner. It should be stressed that, to reduce the computational cost, they employed a technique with a fixed kaon sink operator for the calculation of  $\pi K$  scattering length for  $I = 1/2$  channel and then an exponential factor is introduced to drop the unnecessary  $t$ -dependence appearing due to the fixed kaon sink time [13]. In this work, we will improve this technique by using a ‘‘moving’’ wall source without gauge fixing where the exponential factor is not needed any more. Thus, there is no satisfactory direct lattice calculation for  $I = 1/2$  channel until now.

In the present study, we will use the MILC gauge configurations generated in the presence of  $N_f = 2+1$  flavors of the Asqtad improved [14, 15] staggered dynamical sea quarks [16, 17] to study the  $s$ -wave  $\pi K$  scattering lengths for both  $I = 1/2$  and  $3/2$  channels. Inspired by the exploratory study of  $\pi\pi$  scattering for  $I = 0$  channel in Ref. [18], we will adopt almost same technique but with moving kaon wall source operator without gauge fixing for  $I = 1/2$  and  $3/2$  channels to obtain the reliable accuracy. We calculated all the three diagrams categorized in Ref. [12], and observed a clear signal of attraction for  $I = 1/2$  channel and that of repulsion for  $I = 3/2$  case. Moreover, for  $I = 1/2$  channel, we employ the variational method to isolate the contamination from the excited states. Most of all, we only used the lattice simulation data of our measured  $\pi K$  scattering lengths for both isospin eigenstates to simultaneously extrapolate toward the physical point using the continuum three-flavor  $\chi$ PT at the next-to-leading order. Our lattice simulation results of the scattering lengths for both isospin eigenchannels are in accordance with the experimental reports and theoretical predictions, and can be comparable with other lattice simulations.

This article is organized as follows. In Sec. II we describe the formalism for the calculation of  $\pi K$  scattering lengths including the Lüscher’s formula [19–21] and our computational technique of the modified wall sources for the measurement of  $\pi K$  four-point functions. In Sec. III we will show the simulation parameters and our concrete lattice calculations. We will present our lattice simulation results in Sec. IV, and arrive at our conclusions and outlooks in Sec. V.

## II. METHOD OF MEASUREMENT

In this section, we will briefly review the formulas of the  $s$ -wave scattering length from two-particle energy in a finite box, with emphasis on the formulae for isospin  $I = 1/2$   $\pi K$  system. Also we will present the detailed procedure for extracting the the energies of  $\pi K$  system. Here we follow the original derivations and notations in Refs. [12, 18, 22–24].

### A. $\pi K$ four-point functions

Let us consider the  $\pi K$  scattering of one Nambu-Goldstone pion and one Nambu-Goldstone kaon in the Asqtad-improved staggered dynamical fermion formalism. Using operators  $O_\pi(x_1), O_\pi(x_3)$  for pions at points  $x_1, x_3$ , and operators  $O_K(x_2), O_K(x_4)$  for kaons at points  $x_2, x_4$ , respectively, with the pion and kaon interpolating field operators defined by

$$\begin{aligned} \mathcal{O}_{\pi^+}(\mathbf{x}, t) &= -\bar{d}(\mathbf{x}, t)\gamma_5 u(\mathbf{x}, t), \\ \mathcal{O}_{\pi^0}(\mathbf{x}, t) &= \frac{1}{\sqrt{2}}[\bar{u}(\mathbf{x}, t)\gamma_5 u(\mathbf{x}, t) - \bar{d}(\mathbf{x}, t)\gamma_5 d(\mathbf{x}, t)], \\ \mathcal{O}_{K^0}(\mathbf{x}, t) &= \bar{s}(\mathbf{x}, t)\gamma_5 d(\mathbf{x}, t), \\ \mathcal{O}_{K^+}(\mathbf{x}, t) &= \bar{s}(\mathbf{x}, t)\gamma_5 u(\mathbf{x}, t), \end{aligned} \quad (1)$$

we then represent the  $\pi K$  four-point functions as

$$C_{\pi K}(x_4, x_3, x_2, x_1) = \langle \mathcal{O}_K(x_4) \mathcal{O}_\pi(x_3) \mathcal{O}_K^\dagger(x_2) \mathcal{O}_\pi^\dagger(x_1) \rangle, \quad (2)$$

where  $\langle \dots \rangle$  represents the expectation value of the path integral, which we evaluate using the lattice QCD simulations.

After summing over spatial coordinates  $\mathbf{x}_1, \mathbf{x}_2, \mathbf{x}_3$  and  $\mathbf{x}_4$ , we obtain the  $\pi K$  four-point function in the zero-momentum state,

$$C_{\pi K}(t_4, t_3, t_2, t_1) = \sum_{\mathbf{x}_1} \sum_{\mathbf{x}_2} \sum_{\mathbf{x}_3} \sum_{\mathbf{x}_4} C_{\pi K}(x_4, x_3, x_2, x_1), \quad (3)$$

where  $x_1 \equiv (\mathbf{x}_1, t_1)$ ,  $x_2 \equiv (\mathbf{x}_2, t_2)$ ,  $x_3 \equiv (\mathbf{x}_3, t_3)$ , and  $x_4 \equiv (\mathbf{x}_4, t_4)$ , and  $t$  stands for the time difference, namely,  $t \equiv t_3 - t_1$ .

To avoid the complicated Fierz rearrangement of the quark lines, we choose the creation operators at the time slices which are different by one lattice time spacing as is suggested in Ref. [23], namely, we select  $t_1 = 0, t_2 = 1, t_3 = t$ , and  $t_4 = t + 1$ . In  $\pi K$  system, there are two isospin eigenstates, namely,  $I = 3/2$  and  $I = 1/2$ , we construct the  $\pi K$  operators for these isospin eigenchannels as [12]

$$\begin{aligned} \mathcal{O}_{\pi K}^{I=\frac{1}{2}}(t) &= \frac{1}{\sqrt{3}} \left\{ \sqrt{2} \pi^+(t) K^0(t+1) - \pi^0(t) K^+(t+1) \right\}, \\ \mathcal{O}_{\pi K}^{I=\frac{3}{2}}(t) &= \pi^+(t) K^+(t+1), \end{aligned} \quad (4)$$

where

$$\begin{aligned} \mathcal{O}_{K^0}(t) &= \sum_{\mathbf{x}} \mathcal{O}_{K^0}(\mathbf{x}, t), & \mathcal{O}_{K^+}(t) &= \sum_{\mathbf{x}} \mathcal{O}_{K^+}(\mathbf{x}, t) \\ \mathcal{O}_{\pi^0}(t) &= \sum_{\mathbf{x}} \mathcal{O}_{\pi^0}(\mathbf{x}, t), & \mathcal{O}_{\pi^+}(t) &= \sum_{\mathbf{x}} \mathcal{O}_{\pi^+}(\mathbf{x}, t). \end{aligned} \quad (5)$$

If we assume that the  $u$  and  $d$  quarks have the same mass, only three diagrams contribute to  $\pi K$  scattering amplitudes [12]. The quark line diagrams contributing to  $\pi K$  four-point function denoted in Eq. (3) are displayed in Figure 1, labeling them as direct (D), crossed (C) and

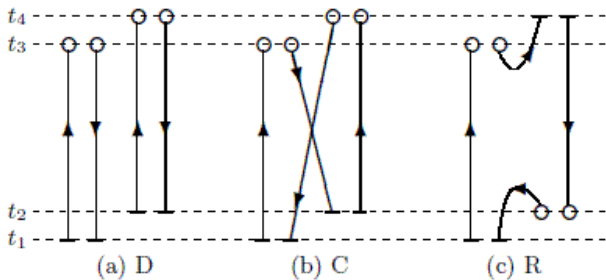


FIG. 1: Diagrams contributing to  $\pi K$  four-point functions. Short bars stand for wall sources. Open circles are sinks for local pion or kaon operators. The thicker lines represent the strange quark lines.

rectangular (R), respectively. The direct and crossed diagrams can be easily evaluated by constructing the corresponding four-point amplitudes for arbitrary values of the time slices  $t_3$  and  $t_4$  using only two wall sources placed at the fixed time slices  $t_1$  and  $t_2$ . However, the rectangular diagram (R) requires another quark propagator connecting the time slices  $t_3$  and  $t_4$ , which make the reliable evaluation of this diagram extremely difficult.

Sasaki et al. solve this problem through the technique with a fixed kaon sink operator to reduce the computational cost [13]. Encouraged by the exploratory works of the  $\pi\pi$  scattering at  $I = 0$  channel in Refs. [18, 23], similarly, we handle this problem by evaluating  $T$  quark propagators on a  $L^3 \times T$  lattice, each propagator, which corresponds to a wall source at the time slice  $t = 0, \dots, T-1$ , is denoted by

$$\sum_{n''} D_{n', n''} G_t(n'') = \sum_{\mathbf{x}} \delta_{n', (\mathbf{x}, t)}, \quad 0 \leq t \leq T-1, \quad (6)$$

where  $D$  is the quark matrix for the staggered Kogut-Susskind quark action. The combination of  $G_t(n)$  which we apply for  $\pi K$  four-point functions is schematically shown in Figure 1, where short bars stand for the position of wall source, open circles are sinks for local pion or kaon operators, and the thicker lines represent the strange quark lines. Likely, the subscript  $t$  in the quark propagator  $G$  represents the position of the wall source.  $D$ ,  $C$ , and  $R$ , are schematically displayed in Figure 1, and we can also expressed them in terms of the quark propagators  $G$ , namely,

$$\begin{aligned} C^D(t_4, t_3, t_2, t_1) &= \sum_{\mathbf{x}_3} \sum_{\mathbf{x}_4} \left\langle \text{Re Tr} \left[ G_{t_1}^\dagger(\mathbf{x}_3, t_3) G_{t_1}(\mathbf{x}_3, t_3) G_{t_2}^\dagger(\mathbf{x}_4, t_4) G_{t_2}(\mathbf{x}_4, t_4) \right] \right\rangle, \\ C^C(t_4, t_3, t_2, t_1) &= \sum_{\mathbf{x}_3} \sum_{\mathbf{x}_4} \left\langle \text{Re Tr} \left[ G_{t_1}^\dagger(\mathbf{x}_3, t_3) G_{t_2}(\mathbf{x}_3, t_3) G_{t_2}^\dagger(\mathbf{x}_4, t_4) G_{t_1}(\mathbf{x}_4, t_4) \right] \right\rangle, \\ C^R(t_4, t_3, t_2, t_1) &= \sum_{\mathbf{x}_2} \sum_{\mathbf{x}_3} \left\langle \text{Re Tr} \left[ G_{t_1}^\dagger(\mathbf{x}_2, t_2) G_{t_4}(\mathbf{x}_2, t_2) G_{t_4}^\dagger(\mathbf{x}_3, t_3) G_{t_1}(\mathbf{x}_3, t_3) \right] \right\rangle, \end{aligned} \quad (7)$$

where daggers mean the conjugation by the even-odd parity  $(-1)^n$  for the staggered Kogut-Susskind quark action, and  $\text{Tr}$  stands for the trace over the color index. The hermiticity properties of the propagator  $G$  are used to eliminate the factors of  $\gamma^5$ .

For  $\pi K$  rectangular diagram in Figure 1(c), it creates the gauge-variant noise [18, 23]. One can reduce the noise by fixing gauge configurations to some gauge (e.g., Coulomb gauge), and select a special wall source to emit only the Nambu-Goldstone pion [25], however, the gauge non-invariant states may contaminate the  $\pi K$  four-point function. Alternatively, we perform the gauge field average without gauge fixing since the gauge dependent fluctuations should neatly cancel out among the lattice configurations. Besides these cancelations, the summation of the gauge-variant terms over the spatial sites of the wall source further suppresses the gauge-variant noise. In our current lattice simulation we found that this method works pretty well.

All three diagrams in Figure 1 are needed to be calculated to study the  $\pi K$  scattering in both  $I = 1/2$  and  $I = 3/2$  channels. Three types of the propagators can be

combined to construct the physical correlation functions for  $\pi K$  states with definite isospin. As it is investigated in Ref. [12], in the isospin limit, the  $\pi K$  correlation function for  $I = 3/2$  and  $1/2$  channels can be expressed as the combinations of three diagrams, namely,

$$\begin{aligned} C_{\pi K}^{I=\frac{1}{2}}(t) &\equiv \left\langle \mathcal{O}_{\pi K}^{I=\frac{1}{2}}(t) | \mathcal{O}_{\pi K}^{I=\frac{1}{2}}(0) \right\rangle = D + \frac{1}{2} N_f C - \frac{3}{2} N_f R, \\ C_{\pi K}^{I=\frac{3}{2}}(t) &\equiv \left\langle \mathcal{O}_{\pi K}^{I=\frac{3}{2}}(t) | \mathcal{O}_{\pi K}^{I=\frac{3}{2}}(0) \right\rangle = D - N_f C, \end{aligned} \quad (8)$$

where the operator  $\mathcal{O}_{\pi K}^I$  denoted in Eq. (4) creates a  $\pi K$  state with total isospin  $I$  and the staggered-flavor factor  $N_f$  is inserted to correct for the flavor degrees of freedom of the Kogut-Susskind staggered fermion [24]. For the pion and kaon operators it is most natural to choose the one in the Nambu-Goldstone channel. This is the choice for our current study.

To calculate the scattering lengths for hadron-hadron scattering on the lattice, or the scattering phase shifts in general, one usually resorts to Lüscher's formula which relates the exact energy level of two hadron states in a finite box to the scattering phase shift in the continuum.

In the case of  $\pi K$  scattering, the  $s$ -wave  $\pi K$  scattering length in the continuum is defined by

$$a_0 = \lim_{k \rightarrow 0} \frac{\tan \delta_0(k)}{k}. \quad (9)$$

$k$  is the magnitude of the center-of-mass scattering momentum which is related to the total energy  $E_{\pi K}^I$  of the  $\pi K$  system with isospin  $I$  in a finite box of size  $L$  by

$$E_{\pi K}^I = \sqrt{m_\pi^2 + k^2} + \sqrt{m_K^2 + k^2}, \quad (10)$$

where the  $m_\pi$  is the pion mass, and  $m_K$  is the kaon mass. We can rewrite Eq. (10) to an elegant form as

$$k^2 = \frac{1}{4} \left( E_{\pi K}^I + \frac{m_\pi^2 - m_K^2}{E_{\pi K}^I} \right)^2 - m_\pi^2. \quad (11)$$

In the absence of the interactions between the  $\pi$  and  $K$  particles,  $k/\tan \delta_0(k) \rightarrow \infty$ , and the energy levels occur at momenta  $k = 2\pi n/L$ , ( $n$  is a integer), corresponding to the single-particle modes in a cubic box.  $\delta_0(k)$  is the  $s$ -wave scattering phase shift, which can be evaluated by the Lüscher's finite size formula [19, 21],

$$\left( \frac{\tan \delta_0(k)}{k} \right)^{-1} = \frac{\sqrt{4\pi}}{\pi L} \cdot \mathcal{Z}_{00} \left( 1, \frac{k^2}{(2\pi/L)^2} \right), \quad (12)$$

where the zeta function  $\mathcal{Z}_{00}(1; q^2)$  is denoted by

$$\mathcal{Z}_{00}(1; q^2) = \frac{1}{\sqrt{4\pi}} \sum_{\mathbf{n} \in \mathbb{Z}^3} \frac{1}{n^2 - q^2}, \quad (13)$$

here  $q = kL/(2\pi)$  is no longer an integer, and  $\mathcal{Z}_{00}(1; q^2)$  can be efficiently calculated by the method described in Ref. [26]. We also discussed this technique in Appendix A, where we extend this discussion to the case with the negative  $q^2$ . In the case of the attractive interaction,  $k^2$  on the bound state has a negative value, therefore  $k$  is pure imaginary, and  $\delta_0(k)$  is no longer physical scattering phase shift [13].  $\mathcal{Z}_{00}(1, q^2)$ , however, still have a real value even for this case, hence  $\tan \delta_0(k)/k$  obtained by Eq. (12) is also real. If  $|k^2|$  is enough small, we can consider  $\tan \delta_0(k)/k$  as the physical scattering length at  $\pi k$  threshold [13].

The energy  $E_{\pi K}^I$  of  $\pi K$  system with isospin  $I$  can be obtained from  $\pi K$  four-point function denoted in Eq. (8) with the large  $t$ . At large  $t$  these correlators will behave as [27, 28]

$$C_{\pi K}^I(t) = Z_{\pi K} \cosh \left[ E_{\pi K}^I \left( t - \frac{T}{2} \right) \right] + (-1)^t Z'_{\pi K} \cosh \left[ E_{\pi K}^I \left( t - \frac{T}{2} \right) \right] + \dots \quad (14)$$

where  $E_{\pi K}^I$  is the energy of the lightest  $\pi K$  state with isospin  $I$ . The terms alternating in sign are a peculiarity of the Kogut-Susskind formulation of the lattice

fermions and correspond to the contributions from intermediate states with opposite parity [27, 28]. The ellipsis suggests the contributions from excited states which are suppressed exponentially.

We should bear in mind that, for the staggered Kogut-Susskind quark action, there are further complications in itself stemming from the non-degeneracy of pions and kaons in the Goldstone and other channels at a finite lattice spacing. Briefly speaking, the contributions of non-Nambu-Goldstone pions and kaons in the intermediate states is exponentially suppressed for large times due to their heavier masses compared to these of the Nambu-Goldstone pion and kaon [18, 23, 24]. Thus, we suppose that  $\pi K$  interpolator does not couple significantly to other  $\pi K$  tastes, and neglect this systematic errors.

In our concrete calculation, we calculated the pion mass  $m_\pi$  and kaon mass  $m_K$  through the methods discussed by the MILC collaboration in Refs. [29, 30] in our previous study [31]. In this work we evaluate total energy  $E_{\pi K}^I$  of  $\pi K$  system with isospin  $I$  from Eq. (14).

In the current study we also evaluate the energy shift  $\delta E_I = E_{\pi K}^I - (m_\pi + m_K)$  from the ratios

$$R^X(t) = \frac{C_{\pi K}^X(0, 1, t, t+1)}{C_\pi(0, t)C_K(1, t+1)}, \quad X = D, C, \text{ and } R, \quad (15)$$

where  $C_\pi(0, t)$  and  $C_K(1, t+1)$  are the pion and kaon two-point functions, respectively. Considering Eq. (8), we can write the amplitudes which project out the  $I = 1/2$  and  $3/2$  isospin eigenstates as

$$\begin{aligned} R_{I=\frac{1}{2}}(t) &= R^D(t) + \frac{1}{2}N_f R^C(t) - \frac{3}{2}N_f R^R(t), \\ R_{I=\frac{3}{2}}(t) &= R^D(t) - N_f R^C(t). \end{aligned} \quad (16)$$

Following the discussions in Ref. [24], we now then can extract the energy shift  $\delta E_I$  from the ratios

$$R_I(t) = Z_I e^{-\delta E_I t} + \dots, \quad (17)$$

where  $Z_I$  stands for wave function factor, which is the ratio of two amplitudes from the  $\pi K$  four-point function and the square of the pion two-point correlator and the kaon two-point correlator, and the ellipsis indicates the terms suppressed exponentially. In  $R_I(t)$ , some of the fluctuations which contribute to both the two-point and four-point correlation functions neatly cancel out, hence, improving the quality of the extraction of the energy shift as compared with what we can obtain from an analysis through the individual correlation functions [11].

For  $I = 3/2$  channel, we can use Eq. (14) or Eq. (17) to extract the energy shifts  $\delta E$ . We have numerically compared the fitting values from two methods, and found well agreement within statistical errors. In fact, using Eq. (17) to extract the energy shift  $\delta E$  has been extensively employed for the study of  $\pi K$  scattering at  $I = 3/2$  case in Ref. [11]. Hence, in this work, we will only present the energy shifts  $\delta E$  calculated by Eq. (17), and then its corresponding scattering lengths.

On the other hand, for  $I = 1/2$  channel, the presence of the kappa resonance is clearly shown in the low energy [13], and therefore it should be necessary for us to separate the ground state contribution from the contamination stemming from the excited states to achieve the reliable scattering length as it is investigated in Ref. [13]. For this purpose, we will construct a  $2 \times 2$  correlation matrix of the time correlation function and diagonalize it to extract the energy of the ground state.

## B. Correlation matrix

For  $I = 1/2$  channel, to separate the contamination from the excited states, we construct a matrix of the time correlation function,

$$C(t) = \begin{pmatrix} \langle 0 | \mathcal{O}_{\pi K}^\dagger(t) \mathcal{O}_{\pi K}(0) | 0 \rangle & \langle 0 | \mathcal{O}_{\pi K}^\dagger(t) \mathcal{O}_\kappa(0) | 0 \rangle \\ \langle 0 | \mathcal{O}_\kappa^\dagger(t) \mathcal{O}_{\pi K}(0) | 0 \rangle & \langle 0 | \mathcal{O}_\kappa^\dagger(t) \mathcal{O}_\kappa(0) | 0 \rangle \end{pmatrix}, \quad (18)$$

where  $\mathcal{O}_\kappa(t)$  is an interpolating operator for the  $\kappa$  meson with zero momentum, and  $\mathcal{O}_{\pi K}(t)$  is an interpolating operator for  $\pi K$  system which is extensively discussed in section II A. The interpolating operator  $\mathcal{O}_\kappa$  employed here is exactly the same as these in our previous studies in Refs. [31–33], the notations adopted here are also the same, but to make this paper self-contained, all the necessary definitions will be also presented below.

### 1. $\kappa$ sector

In our previous studies [31–33], we have presented a detailed procedure to measure kappa correlator  $\langle 0 | \kappa^\dagger(t) \kappa(0) | 0 \rangle$ . To simulate the correct number of quark species, we use the fourth-root trick [34], which automatically performs the transition from four tastes to one taste per flavor for staggered fermion at all orders. We employ an interpolation operator with isospin  $I = 1/2$  and  $J^P = 0^+$  at the source and sink,

$$\mathcal{O}(x) \equiv \frac{1}{\sqrt{n_r}} \sum_{a,g} \bar{s}_g^a(x) u_g^a(x), \quad (19)$$

where  $g$  is the indices of the taste replica,  $n_r$  is the number of the taste replicas,  $a$  is the color indices, and we omit the Dirac-Spinor index. The time slice correlator for the  $\kappa$  meson in the zero momentum state can be evaluated by

$$C_\kappa(t) = \frac{1}{n_r} \sum_{\mathbf{x}, a, b, g, g'} \langle \bar{s}_{g'}^b(\mathbf{x}, t) u_{g'}^b(\mathbf{x}, t) \bar{u}_g^a(\mathbf{0}, 0) s_g^a(\mathbf{0}, 0) \rangle,$$

where  $\mathbf{0}, \mathbf{x}$  are the spatial points of the  $\kappa$  state at source and sink, respectively. After performing Wick contractions of fermion fields, and summing over the taste index,

for the light  $u$  quark Dirac operator  $M_u$  and the  $s$  quark Dirac operator  $M_s$ , we obtain [31]

$$C_\kappa(t) = \sum_{\mathbf{x}} (-)^x \left\langle \text{Tr} [M_u^{-1}(\mathbf{x}, t; 0, 0) M_s^{-1\dagger}(\mathbf{x}, t; 0, 0)] \right\rangle, \quad (20)$$

where  $\text{Tr}$  is the trace over the color index, and  $x = (\mathbf{x}, t)$  is the lattice position.

For the staggered quarks, the meson propagators have the generic single-particle form,

$$\mathcal{C}(t) = \sum_i A_i e^{-m_i t} + \sum_i A'_i (-1)^t e^{-m'_i t} + (t \rightarrow N_t - t), \quad (21)$$

where the oscillating terms correspond to a particle with opposite parity. For  $\kappa$  meson correlator, we consider only one mass with each parity in Eq. (21), namely, in our concrete calculation, our operator is the state with spin-taste assignment  $I \otimes I$  and its oscillating term with  $\gamma_0 \gamma_5 \otimes \gamma_0 \gamma_5$  [31]. Thus, the  $\kappa$  correlator was fit to the following physical model,

$$C_\kappa(t) = b_\kappa e^{-m_\kappa t} + b_{K_A} (-)^t e^{-M_{K_A} t} + (t \rightarrow N_t - t), \quad (22)$$

where  $b_{K_A}$  and  $b_\kappa$  are two overlap factors. In Figure 6, we clearly note this oscillating term.

We should bear in mind that, for the staggered Kogut-Susskind quark action, our  $\kappa$  interpolating operator couples to various tastes as we examined the scalar  $a_0$  and  $\sigma$  mesons in Refs. [35, 36], where we investigated two-pseudoscalar intermediates states (namely, bubble contribution). In Ref. [32], we investigated the extracted  $\kappa$  masses with and without bubble contribution for kappa correlators. We found that there are only about 2% ~ 5% differences in masses, although the bubble contributions are dominant in the  $\kappa$  correlators at large time region. Thus, in the current study, we can reasonably assume that the  $\kappa$  interpolator does not couple remarkably to other tastes, and ignore this systematic errors for the  $\kappa$  sector [33].

### 2. Off-diagonal sector

The calculations of the off-diagonal elements in correlation matrix  $C(t)$  in Eq. (18), namely,  $\langle 0 | \mathcal{O}_{\pi K}^\dagger(t) \mathcal{O}_\kappa(0) | 0 \rangle$  and  $\langle 0 | \mathcal{O}_\kappa^\dagger(t) \mathcal{O}_{\pi K}(0) | 0 \rangle$  are exactly the same as these in our previous study for non-zero momenta in Ref. [33], the notations adopted here are also the same, but to make this paper self-contained, all the necessary definitions will be also presented below.

To avoid the complicated Fierz rearrangement of the quark lines, we choose the creation operators at the time slices which are different by one lattice time spacing as suggested in Ref. [23], namely, we select  $t_1 = 0, t_2 = 1$ , and  $t_3 = t$  for  $\pi K \rightarrow \kappa$  three-point function, and choose  $t_1 = 0, t_2 = t$ , and  $t_3 = t + 1$  for  $\kappa \rightarrow \pi K$  three-point function.

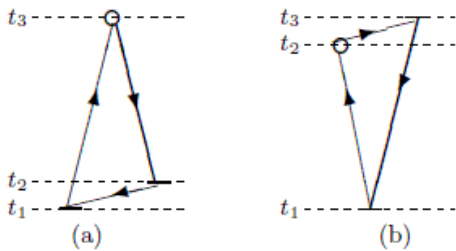


FIG. 2: Diagrams contributing to  $\pi K \rightarrow \kappa$  and  $\kappa \rightarrow \pi K$  three-point functions. Short bars stand for wall sources. The thicker lines represent the strange quark lines. (a) Quark contractions of  $\pi K \rightarrow \kappa$ , where open circle is sink for local kappa operator. (b) Quark contractions of  $\kappa \rightarrow \pi K$ , where open circle is sink for local pion operator.

The quark line diagrams contributing to the  $\kappa \rightarrow \pi K$  and  $\pi K \rightarrow \kappa$  three-point function are plotted in Fig-

ure 2(a) and Figure 2(b), respectively, where short bars stand for the position of wall source, open circles are sinks for local pion or kaon operators, and the thicker lines represent the strange quark lines. Likely, the subscript  $t$  in the quark propagator  $G$  represents the position of the wall source.

The  $\pi K \rightarrow \kappa$  three-point function can be easily evaluated by constructing the corresponding three-point amplitudes for arbitrary values of the time slice  $t_3$  using only two wall sources placed at the fixed time slices  $t_1$  and  $t_2$ . However, the calculation of  $\kappa \rightarrow \pi K$  three-point function is almost the same difficult as that of the rectangular diagram for  $\pi K$  four-point correlator function, since it requires another quark propagator connecting time slices  $t_2$  and  $t_3$ . The  $\kappa \rightarrow \pi K$  and  $\pi K \rightarrow \kappa$  three-point functions are schematically shown in Figure 2, and we can also express them in terms of the quark propagators  $G$ , namely,

$$\begin{aligned} C_{\pi K \rightarrow \kappa}(t_3, t_2, t_1) &= \sum_{\mathbf{x}_3, \mathbf{x}_1} \left\langle \text{Re Tr} [G_{t_1}(\mathbf{x}_3, t_3) G_{t_2}^\dagger(\mathbf{x}_3, t_2) G_{t_3}^\dagger(\mathbf{x}_1, t_1)] \right\rangle, \\ C_{\kappa \rightarrow \pi K}(t_3, t_2, t_1) &= \sum_{\mathbf{x}_2, \mathbf{x}_1} \left\langle \text{Re Tr} [G_{t_1}(\mathbf{x}_2, t_2) G_{t_3}^\dagger(\mathbf{x}_2, t_3) G_{t_3}^\dagger(\mathbf{x}_1, t_1)] \right\rangle. \end{aligned} \quad (23)$$

### C. Extraction of energies

Through calculating the matrix of correlation function  $C(t)$  denoted in Eq. (18), we can separate the ground state from first excited state in a clean way. It is very important to map out “avoided level crossings” between the  $\kappa$  resonance and its decay products (namely,  $\pi$  and  $K$ ) in a finite box volume, because the first excited state is potentially close to the ground state. This makes the extraction of the ground state energy unfeasible if we only utilize a single exponential fit ansatz. Since we can not predict a priori whether our energy eigenvalues are near to the resonance region or not, we find it always safe in practice to adopt the correlation matrix to analyze our lattice simulation data for isospin  $I = 1/2$  channel. To extract the ground state, we follow the variational method [20] and construct a ratio of correlation function matrices as

$$M(t, t_R) = C(t) C^{-1}(t_R), \quad (24)$$

with some reference time slice  $t_R$  [20], which is assumed to be large enough such that the contributions to correlation matrix  $M(t, t_R)$  from the excited states can be neglected, and the lowest two eigenstates dominate the correlation function. The two lowest energy levels can be extracted by a proper fit to two eigenvalues  $\lambda_n(t, t_R)$  ( $n = 1, 2$ ) of matrix  $M(t, t_R)$ . Because here we work on the staggered fermions, and we can easily prove that

$\lambda_n(t, t_R)$  ( $n = 1, 2$ ) behaves as [33]

$$\begin{aligned} \lambda_n(t, t_R) &= A_n \cosh \left[ -E_n \left( t - \frac{T}{2} \right) \right] + \\ &(-1)^t B_n \cosh \left[ -E'_n \left( t - \frac{T}{2} \right) \right], \end{aligned} \quad (25)$$

for a large  $t$ , which mean  $0 \ll t_R < t \ll T/2$  to suppress the excited states and the unwanted thermal contributions. This equation explicitly contains an oscillating term. For the current study, we are only interested in eigenvalue  $\lambda_1(t, t_R)$ , here non-degenerate eigenvalues  $\lambda_1(t, t_R) > \lambda_2(t, t_R)$  are assumed. In practice, we found that the oscillating term in  $\lambda_1(t, t_R)$  is not appreciable for some  $t_R$ , we can also adopt following simple fitting model [33],

$$\lambda_1(t, t_R) = A \cosh(-E(t - T/2)), \quad (26)$$

and the difference between the fitting models of Eq. (25) and Eq. (26) is small. However, to make our extracted ground energy  $E$  for isospin  $I = 1/2$  channel always reliable, in this work, we will present the ground energy  $E$  calculated by Eq. (25), and then its corresponding  $s$ -wave scattering lengths.

### III. LATTICE CALCULATION

#### A. Simulation parameters

We used the MILC lattices with 2+1 dynamical flavors of the Asqtad-improved staggered dynamical fermions, the detailed description of the simulation parameters can be found in Refs. [16, 17]. One thing we must stress that the MILC configurations are generated using the staggered formulation of lattice fermions [37–39] with rooted staggered sea quarks [30] which are hypercubic-smear (HYP-smear) [40–43]. As it was shown in Refs. [44, 45] that HYP-smearing gauge links significantly improves the chiral symmetry.

We analyzed  $\pi K$  four-point functions on the 0.15 fm MILC lattice ensemble of 450  $16^3 \times 48$  gauge configurations with bare quark masses  $am_{ud} = 0.0097$  and  $am_s = 0.0484$  and bare gauge coupling  $10/g^2 = 6.572$ , which has a physical volume approximately 2.5 fm. The inverse lattice spacing  $a^{-1} = 1.358_{-13}^{+35}$  GeV [16, 17]. The mass of the dynamical strange quark is near to its physical value, and the masses of the  $u$  and  $d$  quarks are degenerate. To avoid the contamination from pions and kaons propagating backward in time, periodic boundary condition is applied to the three spatial directions while in the temporal direction, Dirichlet boundary condition is imposed, which reduce the original time extent of 48 down to 24, moreover, it avoids the “fake effects” discussed in Ref. [13].

#### B. Sources for isospin $I = 1/2$ channel

To calculate the  $\pi K$  correlation functions, we use the standard conjugate gradient method (CG) to obtain the required matrix element of the inverse fermion matrix. The calculation of the correlation function for the rectangular diagrams naturally requires us to compute the propagators on all the time slices  $t_s = 0, \dots, T - 1$  of both source and sink, which requires the calculation of 48 separate propagators in our lattice simulations. After averaging the correlator over all 48 possible values, the statistics are greatly improved since we can put the pion source and kaon source at all possible time slices, namely, the correlator  $C_{11}(t)$  is calculated through

$$\begin{aligned} C_{11}(t) &= \left\langle (\pi K)(t) (\pi K)^\dagger(0) \right\rangle \\ &= \frac{1}{T} \sum_{t_s} \left\langle (\pi K)(t + t_s) (\pi K)^\dagger(t_s) \right\rangle, \end{aligned} \quad (27)$$

The best-effort to generate the propagators on all time slices enables us to obtain the correlators with high precision, which is vital to extract the desired scattering phase shifts reliably.

For each time slice, six fermion matrix inversions are required corresponding to the possible 3 color choices for the pion source and kaon source, respectively, and each

inversion takes about one thousand iterations during the CG calculation. Therefore, all together we carry out 288 inversions on a full QCD configuration. As shown follow, this large number of inversions, performed on 450 configurations, provides the substantial statistics needed to resolve the real parts of the  $I = 1/2$  and  $3/2$  amplitudes with reliable accuracy.

In the calculation of the off-diagonal correlator,  $C_{21}(t)$ , the quark line contractions results in a three-point diagram. Since in this three-point diagram the pion field and kaon field are located at the source time slice  $t_s$ ,  $t_s + 1$ , respectively. We calculate the off-diagonal correlator  $C_{21}(t)$  through

$$\begin{aligned} C_{21}(t) &= \left\langle \kappa(t) (\pi K)^\dagger(0) \right\rangle \\ &= \frac{1}{T} \sum_{t_s} \left\langle \kappa(t + t_s) (\pi K)^\dagger(t_s) \right\rangle, \end{aligned} \quad (28)$$

where, again, we sum the correlator over all time slices  $t_s$  and average it. As for the second off-diagonal correlator  $C_{12}(t)$ , the pion field and kaon field are placed at the sink time slices  $t_s + t$  and  $t + t_s + 1$ , respectively, which make the computation of  $C_{12}(t)$  difficult. However, using the relation  $C_{12}(t) = C_{21}^*(t)$ , we can obtain the matrix element  $C_{12}$  for free. As it is studied in Ref. [46], since the sink and source operators are identical for a large number of configurations,  $C(t)$  is a Hermitian matrix. The  $\kappa \rightarrow \pi K$  component agrees with  $\pi K \rightarrow \kappa$  within the error, but the statistical errors of the matrix element  $C_{12}$  should be larger than that of matrix element  $C_{21}$  for a large  $t$ . Therefore, in the following analyses we substitute matrix element  $C_{12}$  by the complex conjugate of matrix element  $C_{21}$ , which is not only to save about 20% computation time, but also significantly to reduce statistical errors.

For the  $\kappa$  correlator,  $C_{22}(t)$ , we have measured the point-to-point correlators with high precision in our previous work [31]. Therefore, we can exploit the available propagators to construct the  $\kappa$ -correlator

$$C_{22}(t) = \frac{1}{T} \sum_{t_s} \left\langle \kappa^\dagger(t + t_s) \kappa(t_s) \right\rangle, \quad (29)$$

where, also, we sum the correlator over all time slices  $t_s$  and average it.

One thing we must stress that, in the calculation of the correlator  $\langle (\pi K)(\pi K)^\dagger \rangle$ , we make our best-efforts to reliably measure the rectangular diagram, since the other two diagrams are relatively easy to evaluate. We found that the rectangular diagram plays a major role in this correlator. Therefore, we get it properly for the  $\pi K$  sector for isospin  $I = 1/2$  channel.

In this work, we also measure two-point correlators for pion and kaon, namely,

$$\begin{aligned} G_\pi(t) &= \langle 0 | \pi^\dagger(t) \pi(0) | 0 \rangle, \\ G_K(t) &= \langle 0 | K^\dagger(t) K(0) | 0 \rangle, \end{aligned} \quad (30)$$

where the  $G_\pi(t)$  is correlation function for the pion with zero momentum, and the  $G_K(t)$  is correlation function for the kaon with zero momentum.

#### IV. SIMULATION RESULTS

In our previous work [47], we have measured the pion and kaon point-to-point correlators. Using these correlators, we can precisely extract the pion mass ( $m_\pi$ ) and kaon mass ( $m_K$ ) [47], which are summarized in Table I. Using the same method discussed in Ref. [48] and the MILC code for calculating the pion decay constants  $f_\pi$ , we precisely extract the pion decay constants  $f_\pi$  [49], which are in agreement with the previous MILC determinations at this same lattice ensemble in Ref. [17]. Here we used all the 631 lattice configurations of this ensemble. We also recapitulated these fitted values in Table I.

TABLE I: Summary of the pion masses, kaon masses and the pion decay constants. The third and fourth blocks show pion masses and kaon masses in lattice units, respectively, and Column five shows the pion decay constants in lattice units. The second block gives pion masses in GeV, where the errors are estimated from both the error on the lattice spacing  $a$  and the statistical errors in Column three.

$am_x$	$m_\pi(\text{GeV})$	$am_\pi$	$am_K$	$af_\pi$
0.00970	0.334(6)	0.2459(2)	0.3962(2)	0.12136(29)
0.01067	0.350(6)	0.2575(2)	0.3996(2)	0.12264(34)
0.01261	0.379(7)	0.2789(2)	0.4066(2)	0.12425(27)
0.01358	0.392(7)	0.2890(2)	0.4101(2)	0.12482(32)
0.01455	0.406(7)	0.2987(2)	0.4134(2)	0.12600(26)
0.01940	0.466(8)	0.3430(2)	0.4300(2)	0.12979(27)

##### A. Diagrams $D, C$ , and $R$

The  $\pi K$  four-point functions are calculated with same lattice configurations using six  $u$  valence quarks, namely,  $am_x = 0.0097, 0.01067, 0.01261, 0.01358, 0.01455$  and  $0.0194$ , where  $m_x$  is the light valence  $u$  quark mass. They all have the same strange sea quark mass  $am_s = 0.0426$ , which is fixed at its physical value [17].

In Figure 3 the individual ratios, which are defined in Eq. (15) corresponding to the diagrams in Figure 1,  $R^X$  ( $X = D, C$  and  $R$ ) are displayed as the functions of  $t$  for  $am_x = 0.0097$ . We can note that diagram  $D$  makes the biggest contribution, then diagram  $C$ , and diagram  $R$  makes the smallest contribution. The calculation of the amplitudes for the rectangular diagram stands for our principal work. Clear signals observed up to  $t = 20$  for the rectangular amplitude demonstrate that the method of the moving wall source without gauge fixing used here is practically applicable.

The values of the direct amplitude  $R^D$  are quite close to unity, indicating that the interaction in this channel is very weak. The crossed amplitude, on the other hand, increases linearly, which implies a repulsion in  $I = 3/2$  channel. After an initial increase up to  $t \sim 4$ , the rectangular amplitude exhibits a roughly linear decrease up

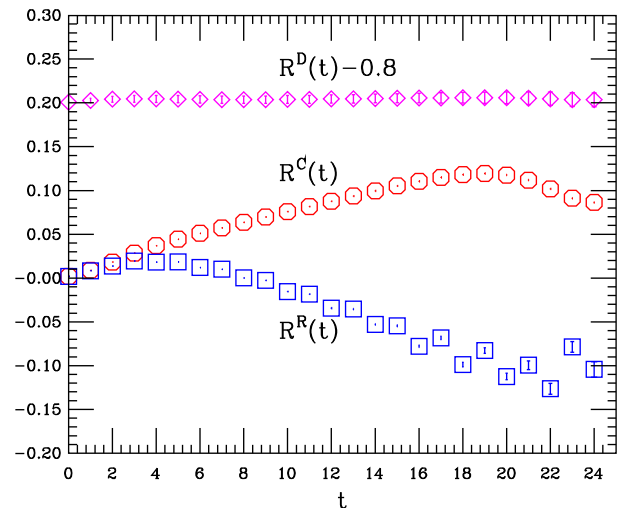


FIG. 3: (color online). Individual amplitude ratios  $R^X(t)$  of the  $\pi K$  four-point function calculated through the moving wall source without gauge fixing as the functions of  $t$  for  $am_x = 0.0097$ . Direct diagram (magenta diamonds) shifted by 0.8, crossed diagram (red octagons) and rectangular diagram (blue squares).

to  $t \sim 20$ , which suggests an attractive force between the pion and kaon in  $I = 1/2$  channel. Furthermore, the magnitude of the slope is similar to that of the crossed amplitude but with opposite sign. These features are what we eagerly expected from the theoretical predictions [6, 24]. We can observe that the crossed and rectangular amplitudes have the same value at  $t = 0$ , and the close values for small  $t$ . Because our analytical expressions in Eq. (7) for the two amplitudes coincide at  $t = 0$ , they should behave similarly until the asymptotic  $\pi K$  state is reached.

In Figure 4, we display the ratio  $R_I(t)$  projected onto the isospin  $I = 1/2$  and  $3/2$  channels for  $am_x = 0.0097$ , which are denoted in Eq. (16). A decrease of the ratio of  $R_{I=3/2}(t)$  indicates a positive energy shift and hence a repulsive interaction for  $I = 3/2$  channel, while an increase of  $R_{I=1/2}(t)$  suggests a negative energy shift and hence an attraction for  $I = 1/2$  channel. A dip at  $t = 3$  for  $I = 1/2$  channel can be clearly observed [23]. The systematically oscillating behavior for  $I = 1/2$  channel in the large time region is also clearly observed, which is a typical characteristic of the Kogut-Susskind formulation of lattice fermions and corresponds to the contributions from the intermediate states of the opposite parity [27, 28], this also clearly indicates the existence of the contaminations from other states rather than the pion-kaon scattering state [13]. Therefore, to isolate the potential contaminations, we will use the variational method [20] to analyze the lattice simulation data. As for  $I = 3/2$  channel, this oscillating characteristic is not appreciable, we will use the traditional method, namely, using Eq. (17) to compute the energy shift  $\delta E$  and then calculate the corresponding scattering length.



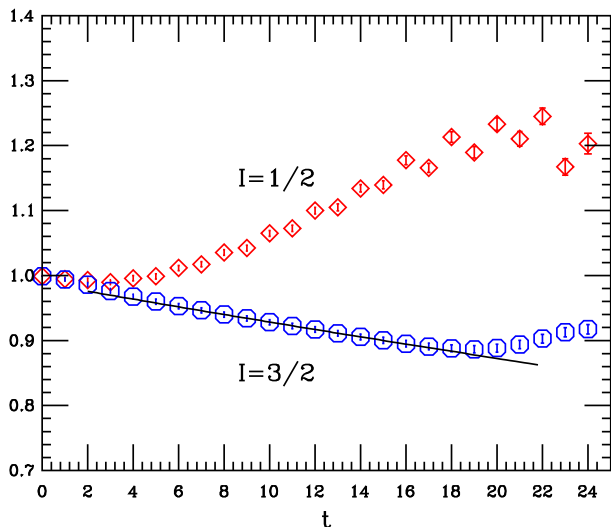


FIG. 4: (color online).  $R_I(t)$  for  $\pi K$  four-point function at zero momenta calculated by the moving wall source without gauge fixing as the functions of  $t$  for  $am_x = 0.0097$ . Solid line in  $I = 3/2$  is exponential fits for  $7 \leq t \leq 16$ .

### B. Fitting analyses for $I = 3/2$ channel

According to our discussions in Section II, in this work, we will make use of Eq. (17) to extract the energy shift  $\delta E$  for  $I = 3/2$  channel. Then we insert these energy shifts into the Eqs. (9) and (12) to obtain the corresponding  $s$ -wave scattering lengths. Therefore, properly extracting the energy shifts is a crucial step to our final results in this paper. A convincing way to analyze our lattice simulation data is with the “effective energy shift” plots, a variant of the effective mass plots, where the propagators were fit with varying minimum fitting distances  $D_{\min}$ , and with the maximum distance  $D_{\max}$  either at the midpoint of the lattice or where the fractional statistical errors exceeded about 20% for two successive time slices. For each valence quark  $m_x$ , the effective energy shift plots as a function of minimum fitting distance  $D_{\min}$  for  $I = 3/2$  channel are shown in Figure 5. The central value and uncertainty of each parameter was determined by the jackknife procedure over the ensemble of gauge configurations.

The energy shifts  $a\delta E$  of  $\pi K$  system for  $I = 3/2$  channel are extracted from the “effective energy shift” plots, and the energy shifts were selected by looking for a combination of a “plateau” in the energy as a function of the minimum distance  $D_{\min}$ , and a good confidence level (namely,  $\chi^2$ ) for the fit. We found that the effective energy shifts for  $I = 3/2$  channel have only relative small errors within broad minimum time distance region  $5 \leq D_{\min} \leq 10$  and are taken to be quite reliable.

We utilize the exponential physical fitting model in Eq. (17) to extract the desired energy shifts for  $I = 3/2$  channel. In Figure 4 we display the ratio  $R_I(t)$  projected onto the  $I = 1/2$  and  $3/2$  channels for  $am_x = 0.0097$ ,

where we can watch the fitted functional form as compared with the lattice simulation data for  $I = 3/2$  channel. For the other five light  $u$  valence quarks, we obtain the similar results, therefore we do not show these ratio  $R_I(t)$  plots here. The fitted values of the energy shifts,  $\delta E_I$  in lattice units and wave function factor  $Z_I$  for  $I = 3/2$  channel are summarized in Table II. The wave function  $Z$  factors are pretty close to unity and the  $\chi^2/\text{dof}$  is quite small for  $I = 3/2$  channel, indicating the values of the extracted scattering lengths are substantially reliable.

TABLE II: Summary of the lattice simulation results for the energy shifts in lattice units for  $I = 3/2$  channel. The third block shows the energy shifts in the lattice unit, Column four shows the wave function factors  $Z$ , Column five shows the time range for the chosen fit, and Column six shows the number of degrees of freedom (dof) for the fit. All errors are calculated from jackknife.

Isospin	$am_x$	$a\delta E$	$Z$	Range	$\chi^2/\text{dof}$
$I = \frac{3}{2}$	0.00970	0.00621(53)	0.9880(59)	7 – 16	0.0536/8
	0.01067	0.00615(52)	0.9893(58)	7 – 16	0.0395/8
	0.01261	0.00602(50)	0.9914(56)	7 – 16	0.0226/8
	0.01358	0.00595(49)	0.9923(55)	7 – 16	0.0176/8
	0.01455	0.00589(48)	0.9930(54)	7 – 16	0.0142/8
	0.01940	0.00561(45)	0.9958(50)	7 – 16	0.0067/8

Now we can insert these energy shifts in Table II into the Eqs. (9) and (12) to obtain the corresponding  $s$ -wave scattering lengths. The center-of-mass scattering momentum  $k^2$  in GeV calculated by Eq. (11), from which we can easily estimate its statistical errors. Once we obtain the values of  $k^2$ , the  $s$ -wave scattering lengths  $a_0$  in lattice units can be obtained through Eqs. (9) and (12). All of these values are summarized in Table III. Here we utilize pion masses and kaon masses given in Table I. The errors of the center-of-mass scattering momentum  $k$  and the  $s$ -wave scattering lengths come from the statistical errors of the energy shifts energies  $\delta E$ , pion mass  $m_\pi$  and kaon mass  $m_K$ .

TABLE III: Summary of the lattice simulation results of the  $s$ -wave scattering lengths for  $I = 3/2$  channel. The third block shows the center-of-mass scattering momentum  $k^2$  in GeV, Column four shows the  $s$ -wave scattering lengths in lattice units, and Column five shows the pion mass times scattering lengths.

Isospin	$am_x$	$k^2[\text{GeV}^2]$	$a_0$	$m_\pi a_0$
$I = \frac{3}{2}$	0.00970	0.00350(27)	-0.558(55)	-0.137(13)
	0.01067	0.00357(28)	-0.569(55)	-0.146(14)
	0.01261	0.00366(30)	-0.582(55)	-0.162(15)
	0.01358	0.00374(30)	-0.593(56)	-0.171(16)
	0.01455	0.00379(34)	-0.600(60)	-0.179(18)
	0.01940	0.00396(37)	-0.624(62)	-0.214(21)

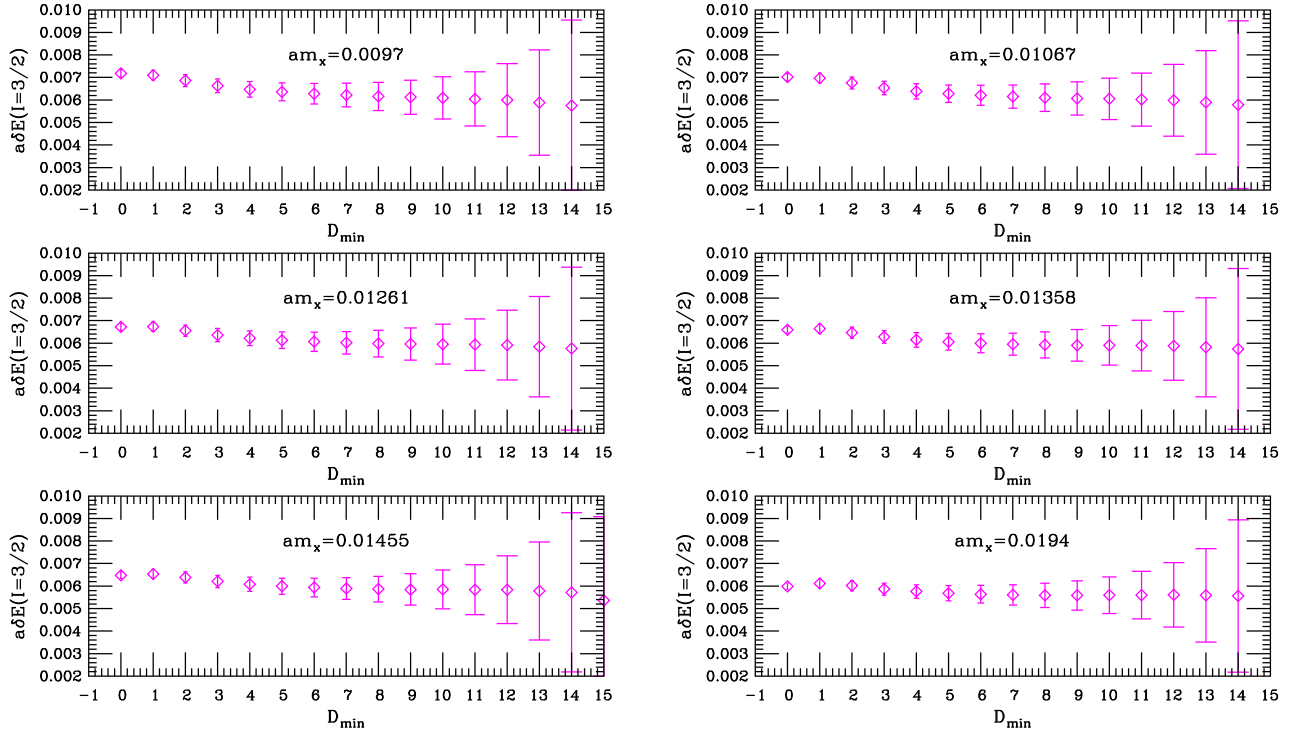


FIG. 5: (color online). The effective  $\pi K$  energy shift plots,  $a\delta E$  as the functions of the minimum fitting distance  $D_{\min}$  in the fit for  $I = 3/2$  channel. The effective  $\pi K$  energy shift plots for  $I = 3/2$  channel have only relative small errors within a broad minimum distance region  $5 \leq D_{\min} \leq 10$ .

### C. Fitting analyses for $I = 1/2$ channel

In Figure 6, we show the real parts of the diagonal components ( $\pi K \rightarrow \pi K$  and  $\kappa \rightarrow \kappa$ ) and the real part of the off-diagonal component  $\pi K \rightarrow \kappa$  of the correlation function  $C(t)$  denoted in Eq. (18). Since  $C(t)$  is a Hermitian matrix, we will substitute the off-diagonal component  $\kappa \rightarrow \pi K$  by  $\pi K \rightarrow \kappa$  to reduce statistical errors in the following analyses.

We calculate two eigenvalues  $\lambda_n(t, t_R)$  ( $n = 1, 2$ ) for the matrix  $M(t, t_R)$  in Eq. (24) with the reference time  $t_R = 7$ . In this work, we are only interested in the eigenvalue  $\lambda_1(t, t_R)$ <sup>1</sup>. In Figure 7 we plot our lattice results for  $\lambda_1(t, t_R)$  for each valence quark  $m_x$  in a logarithmic scale as the functions of  $t$  together with a correlated fit to the asymptotic form given in Eq. (25). From these fits we then extract the energies that will be used to determine the  $s$ -wave scattering lengths.

To extract the energies reliably, we must take two major sources of the systematic errors into consideration. One arises from the excited states which affect the correlator in low time slice region. The other one stems from the thermal contributions which distort the correlator in high time slice region. By denoting a fitting range

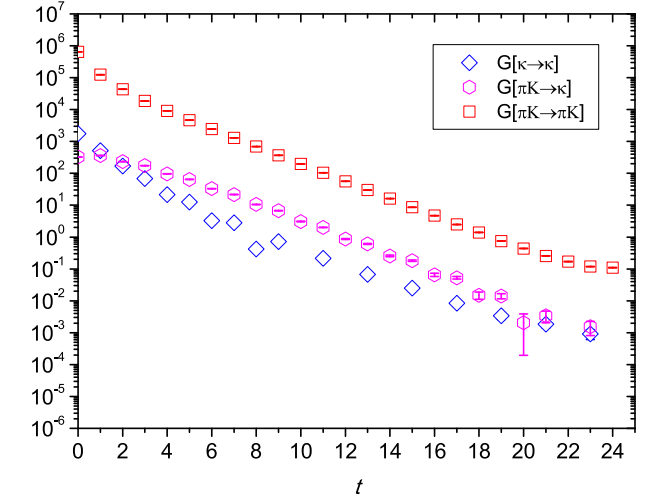


FIG. 6: (color online). Real parts of the diagonal components ( $\pi K \rightarrow \pi K$  and  $\kappa \rightarrow \kappa$ ) and the real part of the off-diagonal component  $\pi K \rightarrow \kappa$  of the time correlation function  $C(t)$ . Occasional points with negative central values for the diagonal component  $\kappa \rightarrow \kappa$  and the off-diagonal component  $\pi K \rightarrow \kappa$  are not plotted.

$[t_{\min}, t_{\max}]$  and varying the values of the  $t_{\min}$  and  $t_{\max}$ , we can control these systematic errors. In our concrete fitting, we take  $t_{\min}$  to be  $t_R + 1$  and increase the reference time slice  $t_R$  to suppress the excited state contaminations. Moreover, we select  $t_{\max}$  to be sufficiently far

<sup>1</sup> In our previous study [33], we have preliminarily examined the behavior of  $\lambda_2(t, t_R)$ .

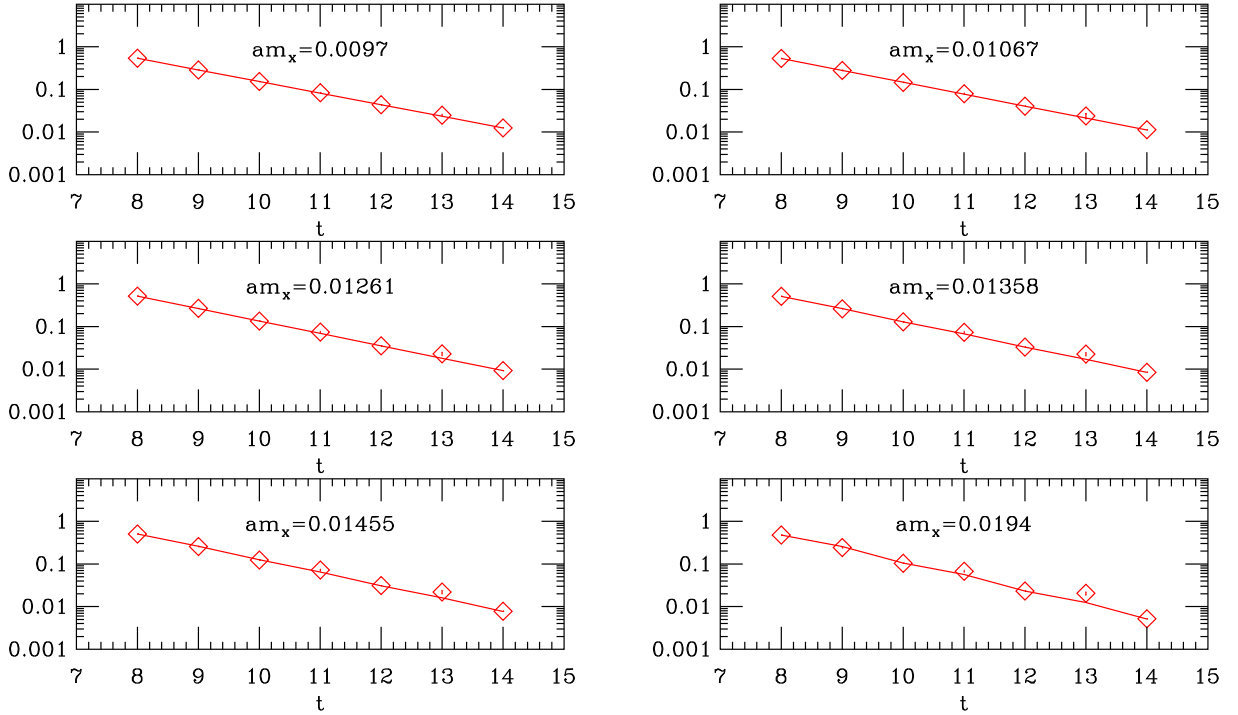


FIG. 7: (color online). The lattice results for  $\lambda_1(t, t_R)$  for each valence quark  $m_x$  in a logarithmic scale as the functions of  $t$  at  $I = 1/2$  channel are shown. The solid lines are correlated fits to Eq. (25), from which the energy eigenvalues are extracted.

away from the time slice  $t = T/2$  to avoid the unwanted thermal contributions. The fitting parameters  $t_R$ ,  $t_{\min}$  and  $t_{\max}$  are tabulated in Table IV. The corresponding fitting results in the reasonable values of  $\chi^2/\text{dof}$ . The  $\chi^2/\text{dof}$  together with the fit results for the energies for the ground state  $aE$  are also listed in Table IV.

TABLE IV: Summary of the lattice simulation results for the fitted values of the energy eigenvalues for the ground state for  $I = 1/2$  channel. The third block shows the energy for the ground state in lattice units. In the table we list the reference time  $t_R$ , the lower and upper bound of the fitting range,  $t_{\min}$  and  $t_{\max}$ , the number of degrees of freedom (dof) for the fit quality  $\chi^2/\text{dof}$ . All errors are calculated from jackknife.

Isospin	$am_x$	$aE$	$t_R$	$t_{\min}$	$t_{\max}$	$\chi^2/\text{dof}$
$I = \frac{1}{2}$	0.00970	0.6260(6)	7	8	14	2.37/3
	0.01067	0.6412(7)	7	8	14	2.83/3
	0.01261	0.6694(10)	7	8	14	3.63/3
	0.01358	0.6828(10)	7	8	14	4.55/3
	0.01455	0.6952(11)	7	8	14	5.57/3
	0.01940	0.7561(12)	7	8	14	13.1/3

Now we can insert these energies in Table IV into the Eqs. (9) and (12) to obtain the scattering lengths. The center-of-mass scattering momentum  $k^2$  in GeV calculated by Eq. (11) and thence the corresponding  $s$ -wave scattering lengths in lattice units obtained through Eqs. (9) and (12) are summarized in Table V. Here we use the pion masses and kaon masses given in Table I.

The errors of the center-of-mass scattering momentum  $k$  and the  $s$ -wave scattering lengths are calculated from the statistic errors of the energy shifts energies  $\delta E$ , pion mass  $m_\pi$  and kaon mass  $m_K$ .

TABLE V: Summary of the lattice simulation results of the  $s$ -wave scattering lengths for  $I = 1/2$  channel. The third block shows the center-of-mass scattering momentum  $k^2$  in GeV, Column four shows the scattering lengths in lattice units, and Column five shows the pion mass times scattering lengths.

Isospin	$am_x$	$k^2[\text{GeV}^2]$	$a_0$	$m_\pi a_0$
$I = \frac{1}{2}$	0.00970	-0.00884(27)	2.32(29)	0.543(34)
	0.01067	-0.00904(29)	2.37(28)	0.588(38)
	0.01261	-0.00956(42)	2.34(29)	0.690(65)
	0.01358	-0.01010(47)	2.69(30)	0.778(78)
	0.01455	-0.01075(52)	2.56(37)	0.887(94)
	0.01940	-0.01343(68)	2.94(55)	1.498(181)

To examine the effects of the contaminations from the excited states for  $I = 1/2$  channel, we denote the ratios of  $C_{00}(t)$  and  $\text{EV}[C^{-1}(t_R)C(t)]_{00}$  which is the lowest eigenvalue of  $C^{-1}(t_R)C(t)$ , to the  $\pi K$  correlator [13],

$$R_0(t) \equiv \frac{C_{00}(t)}{C_{00}(t_R)},$$

$$D_0(t) \equiv \text{EV}[C^{-1}(t_R)C(t)]_{00}. \quad (31)$$

In the upper panel of Figure 8, we show  $R_0(t)$  (magenta diamonds) and  $D_0(t)$  (blue octagons) at  $m_\pi \simeq 0.33$  GeV.

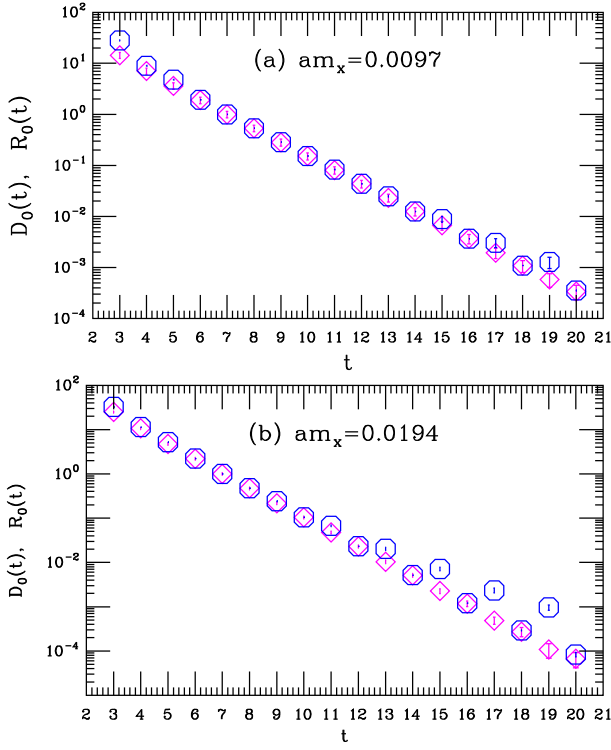


FIG. 8: (color online).  $R_0(t)$  (magenta diamonds) and  $D_0(t)$  (blue octagons) at (a)  $am_x = 0.0097$  or  $m_\pi \simeq 0.33$  GeV and (b)  $am_x = 0.0194$  or  $m_\pi \simeq 0.466$  GeV for  $I = 1/2$  channel.

We can note that the difference of two ratios is small. This suggests that the contamination from the excited states is negligible at this light quark mass. However, from the bottom panel of Figure 8, we observe that the contamination from the excited states is not negligible at  $m_\pi \simeq 0.466$  GeV, and the diagonalization obviously changes the characteristics of the ratio, since the  $\pi K$  interpolative operator for  $I = 1/2$  channel has a large overlap with the excited states [13]. Therefore, we further confirmed that the separation of the contamination from the excited states is absolutely necessary for the heavy quark masses [13] when we study the  $\pi K$  scattering for  $I = 1/2$  channel.

Using the fitting models discussed in Ref. [29], we extract the pion and kaon masses [47]. And using the fitting model in Eq (22), we calculate the kappa mass [32].

$$\begin{aligned}
 a_0^{I=\frac{3}{2}} &= \frac{\mu_{\pi K}}{4\pi f_\pi^2} \left\{ -1 + \frac{32m_\pi m_K}{f_\pi^2} L_{\pi K}(\Lambda_\chi) - \frac{16m_\pi^2}{f_\pi^2} L_5(\Lambda_\chi) + \frac{1}{16\pi^2 f_\pi^2} \chi_{\pi K}^{I=\frac{3}{2}}(\Lambda_\chi, m_\pi, m_K) \right\}, \\
 a_0^{I=\frac{1}{2}} &= \frac{\mu_{\pi K}}{4\pi f_\pi^2} \left\{ 2 + \frac{32m_\pi m_K}{f_\pi^2} L_{\pi K}(\Lambda_\chi) + \frac{32m_\pi^2}{f_\pi^2} L_5(\Lambda_\chi) + \frac{1}{16\pi^2 f_\pi^2} \chi_{\pi K}^{I=\frac{1}{2}}(\Lambda_\chi, m_\pi, m_K) \right\}, \quad (32)
 \end{aligned}$$

where we plugged in the pion mass  $m_\pi$ , the kaon mass  $m_K$ , and the pion decay constant  $f_\pi$ , which are summa-

In Figure 9, we display  $m_\kappa, m_K, m_\pi$ , and  $\pi K$  threshold  $m_{\pi+K}$  in lattice units as the functions of the pion mass  $m_\pi$ . We observe that, as the valence quark mass increases,  $\pi K$  threshold grows faster than  $\kappa$  mass and, as a consequence, for the heavy quark masses,  $\pi K$  threshold is close to the  $\kappa$  mass. In Figure 9, we can clearly note that  $\pi K$  threshold is very close to the  $\kappa$  mass for light quark mass  $am_x = 0.0097$ . This can be in part explained why the separation of the contamination from the excited states is indispensable for the large quark masses [13].

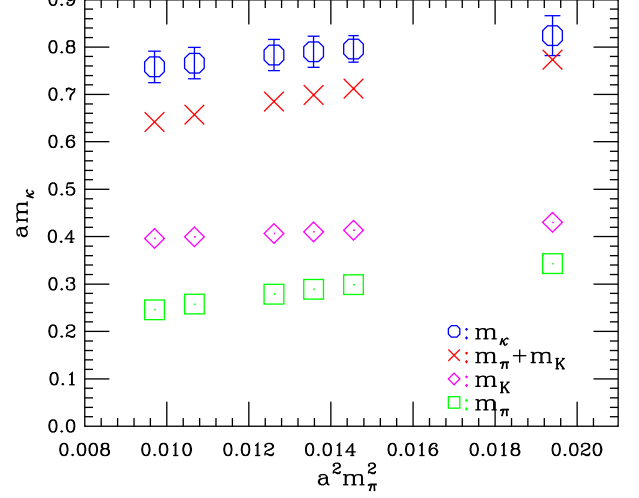


FIG. 9: (color online). Characteristics of  $m_\kappa, m_K, m_\pi$  and  $m_{\pi+K}$  in lattice units as the functions of the pion mass.

#### D. Chiral extrapolations and scattering length

In the present study, we employ a reasonable small pion masses  $m_\pi$ , namely,  $m_\pi = 0.330 - 0.466$  GeV, which are still considerably larger than its physical ones, therefore, we need to extrapolate the  $s$ -wave  $\pi K$  scattering lengths toward the physical point. For this purpose, we employ the formula predicted by SU(3) chiral perturbation theory to next-to-leading order (NLO) [6, 8, 11, 13, 50]. In SU(3) chiral perturbation theory at NLO, we provide the continuum SU(3)  $\chi$ Pt forms of  $a_0^{I=\frac{3}{2}}$  and  $a_0^{I=\frac{1}{2}}$ , which can be directly constructed from Refs. [8, 11, 13],

rized Table I.  $L_5(\Lambda_\chi)$  and  $L_{\pi K}(\Lambda_\chi) \equiv 2L_1 + 2L_2 + L_3 -$

$2L_4 - L_5/2 + 2L_6 + L_8$  are low energy constants defined in Ref. [51] at the chiral symmetry breaking scale  $\Lambda_\chi$ . We should bear in mind that the expressions in Eq. (32) are written in terms of full  $f_\pi$ , and not its chiral limit value.

The  $\chi_{\pi K}^{I=3/2}(\Lambda_\chi, m_\pi, m_K)$  and  $\chi_{\pi K}^{I=1/2}(\Lambda_\chi, m_\pi, m_K)$  are the known functions at NLO which clearly depend upon the chiral scale  $\Lambda_\chi$  with chiral logarithm terms, namely,

$$\begin{aligned}\chi_{\pi K}^{I=3/2}(\Lambda_\chi, m_\pi, m_K) &= \kappa_\pi \ln \frac{m_\pi^2}{\Lambda_\chi^2} + \kappa_K \ln \frac{m_K^2}{\Lambda_\chi^2} + \kappa_\eta \ln \frac{m_\eta^2}{\Lambda_\chi^2} + \frac{86}{9} m_K m_\pi + \kappa_{\tan} \arctan \left( \frac{2(m_K - m_\pi)}{m_K + 2m_\pi} \sqrt{\frac{m_K + m_\pi}{2m_K - m_\pi}} \right), \\ \chi_{\pi K}^{I=1/2}(\Lambda_\chi, m_\pi, m_K) &= \kappa'_\pi \ln \frac{m_\pi^2}{\Lambda_\chi^2} + \kappa'_K \ln \frac{m_K^2}{\Lambda_\chi^2} + \kappa'_\eta \ln \frac{m_\eta^2}{\Lambda_\chi^2} + \frac{86}{9} m_K m_\pi + \frac{3}{2} \kappa_{\tan} \arctan \left( \frac{2(m_K - m_\pi)}{m_K + 2m_\pi} \sqrt{\frac{m_K + m_\pi}{2m_K - m_\pi}} \right) \\ &\quad + \kappa'_{\tan} \arctan \left( \frac{2(m_K + m_\pi)}{m_K - 2m_\pi} \sqrt{\frac{m_K - m_\pi}{2m_K + m_\pi}} \right),\end{aligned}\quad (33)$$

with

$$\begin{aligned}\kappa_\pi &= \frac{11m_K m_\pi^3 + 8m_\pi^2 m_K^2 - 5m_\pi^4}{2(m_K^2 - m_\pi^2)}, \\ \kappa_K &= -\frac{67m_K^3 m_\pi - 8m_\pi^3 m_K + 23m_K^2 m_\pi^2}{9(m_K^2 - m_\pi^2)}, \\ \kappa_\eta &= \frac{24m_\pi m_K^3 - 5m_K m_\pi^3 + 28m_K^2 m_\pi^2 - 9m_\pi^4}{18(m_K^2 - m_\pi^2)}, \\ \kappa_{\tan} &= -\frac{16m_K m_\pi}{9} \frac{\sqrt{2m_K^2 + m_K m_\pi - m_\pi^2}}{m_K - m_\pi}, \\ \kappa'_\pi &= \frac{11m_K m_\pi^3 - 16m_K^2 m_\pi^2 + 10m_\pi^4}{2(m_K^2 - m_\pi^2)}, \\ \kappa'_K &= -\frac{67m_K^3 m_\pi - 8m_\pi^3 m_K - 46m_K^2 m_\pi^2}{9(m_K^2 - m_\pi^2)}, \\ \kappa'_\eta &= \frac{24m_\pi m_K^3 - 5m_K m_\pi^3 - 56m_K^2 m_\pi^2 + 18m_\pi^4}{18(m_K^2 - m_\pi^2)}, \\ \kappa'_{\tan} &= \frac{8m_K m_\pi}{9} \frac{\sqrt{2m_K^2 - m_K m_\pi - m_\pi^2}}{m_K + m_\pi}.\end{aligned}\quad (34)$$

In this work, we did not measure the  $\eta$  mass ( $m_\eta$ ), alternatively, we utilize the Gell-Mann-Okubo mass-relation to determine  $\eta$ -mass. To improve the  $\chi$ Pt fit, in principle, we can include all the lattice simulation data of the  $\pi K$  scattering lengths for both  $I = 1/2$  and  $3/2$  channels to perform the simultaneous fitting. However, the fit with the data of the scattering lengths for  $I = 1/2$  channel in  $m_\pi \geq 0.392$  GeV significantly increases  $\chi^2/\text{dof}$ , so we only use the scattering lengths for  $I = 1/2$  channel in  $m_\pi < 0.392$  GeV. The fitting results of  $\pi K$  scattering lengths,  $m_\pi a_0^{I=3/2}$  and  $m_\pi a_0^{I=1/2}$  are plotted by the dotted lines as the functions of  $m_\pi^2$  in Figure 10. The dotted lines are the chiral extrapolation of the scattering lengths for both isospin eigenstates. The fit parameters  $L_{\pi K}$ ,  $L_5$ , and the scattering lengths  $m_\pi a_0$  at the physical points (namely,  $m_\pi = 0.140$  GeV,  $m_K = 0.494$  GeV) [52] are also summarized in Table VI, where the chiral scale  $\Lambda_\chi$  is taken as the physical  $\eta$  mass, namely,  $\Lambda_\chi = 0.548$  GeV [52] as it is done in Ref. [48]. The cyan diamond points in Figure 10 shows the values of the physical scat-

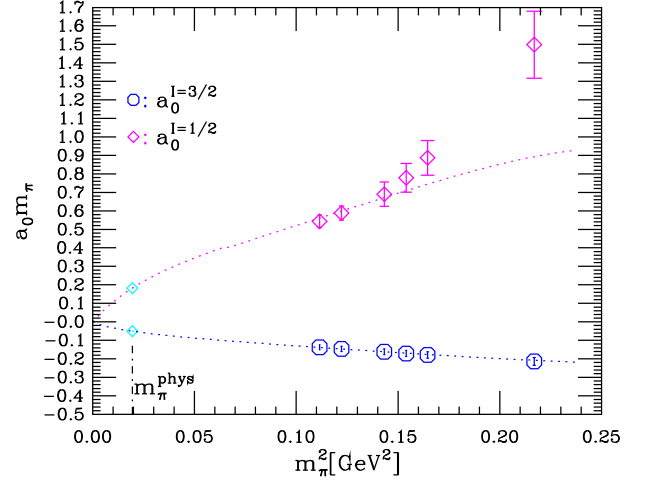


FIG. 10:  $m_\pi^2$ -dependence of the  $\pi K$  scattering lengths  $m_\pi a_0$  for both  $I = 1/2$  and  $I = 3/2$  channels. The dotted lines give the SU(3)  $\chi$ Pt predictions at NLO. The cyan diamond point indicate its physical values.

tering lengths. From Figure 10, we note that our lattice simulation results for  $I = 3/2$  scattering length agrees well with the one-loop formula, while scattering lengths for  $I = 1/2$  channel have a large error, and is in reasonable agreement with the SU(3)  $\chi$ Pt at NLO.

TABLE VI: The fitted  $s$ -wave scattering lengths  $m_\pi a_0$  at the physical point ( $m_\pi = 0.140$  GeV,  $m_K = 0.494$  GeV). The chiral scale  $\Lambda_\chi$  is taken as the physical  $\eta$  mass.

$\chi^2/\text{dof}$	$10^3 \cdot L_{\pi K}$	$10^3 \cdot L_5$	$m_\pi a_0^{I=3/2}$	$m_\pi a_0^{I=1/2}$
0.287/7	1.48(5)	1.06(14)	-0.0505(19)	0.1827(37)

The fitted value of the  $L_5$  is reasonable consistent with the value evaluated by PACS-CS collaboration [53], and is smaller than the corresponding result evaluated by MILC collaboration [48] and NPLQCD collaboration [11]. The fitted value of  $L_{\pi K}$  is also smaller than

the result evaluated by NPLQCD collaboration [11]. The  $s$ -wave  $\pi K$  scattering lengths for both  $I = 1/2$  and  $3/2$  channels are in agreement with the other lattice studies [10–13].

## V. SUMMARY AND OUTLOOK

In the present study, we carried out a direct lattice QCD calculation of the  $s$ -wave  $\pi K$  scattering lengths for both isospin  $I = 1/2$  and  $3/2$  channels, where the rectangular diagram plays a crucial role, for the MILC “medium” coarse ( $a = 0.15$  fm) lattice ensemble in the presence of  $2 + 1$  flavors of the Asqtad improved staggered dynamical sea quarks, generated by the MILC collaboration. We employed almost same technique in Ref. [18] but with the moving wall sources without gauge fixing to obtain the reliable precision. We calculated all the three diagrams categorized in Ref. [12], and observed a clear signal of the attraction for  $I = 1/2$  channel and that of repulsion for  $I = 3/2$  channel, respectively. Moreover, for  $I = 1/2$  channel, we employed the variational method to isolate the contamination from the excited states. We further confirmed that the separation of the contamination is absolutely necessary for the heavy quark masses [13] when we study  $\pi K$  scattering in  $I = 1/2$  channel. Simultaneously extrapolating our lattice simulation data of the  $s$ -wave scattering lengths for both isospin eigenstates to the physical point gives the scattering lengths  $m_\pi a_{3/2} = -0.0505(19)$  and  $m_\pi a_{1/2} = 0.1827(37)$  for the  $I = 3/2$  and  $1/2$  channels, respectively, which are in accordance with the current theoretical predictions to one-loop levels and the present experimental reports, and can be comparable with the other lattice studies [10–13].

A clear signal can be seen for long time separation range in the rectangular diagram of the  $\pi K$  scattering. Reducing the noise by performing the calculation on a larger volume or the smaller pion mass could further improve the signal to noise ratio for the rectangular diagram, and therefore obtain better results for the scattering length in  $I = 1/2$  channel [13]. Moreover, the behavior near the chiral limit is strongly affected by the chiral logarithm term, so giving an evaluation without the long chiral extrapolation is highly desirable to ensure the convergence of the chiral expansion [13]. Furthermore,  $\tan \delta_0(k)/k$  in the low-momentum limit must be evaluated by the systematic studies with the different volumes and boundary conditions [13]. For these purposes, we are planning a series of lattice simulations on MILC coarse, fine, and superfine lattice ensembles with concentrating on the lightest accessible values of the quark masses, namely, in  $m_\pi < 300$  MeV. We anticipate that these future tasks should make the calculation of the rectangular diagram more reliable.

It is well-known that  $\pi K$  scattering at  $I = 1/2$  channel is a more challenging and interesting channel phenomenologically due to the existence of kappa resonance. The study of the  $s$ -wave  $\pi K$  scattering at zero momentum is

just first step in the study of the hadron interactions including  $s$ -quarks. However, it is particularly encouraging that  $\pi K$  scattering for  $I = 1/2$  channel can be reliably calculated by the moving wall sources without gauge fixing in spite of the essential difficulties of the calculation of the four-point functions, especially rectangular diagram. It raises a prospect that this technique can be successfully employed to investigate the  $\kappa$  resonance, and so on.

In our previous work [31], we have precisely evaluated the  $\kappa$  mass, and found that the decay  $\kappa \rightarrow \pi K$  is only allowed kinematically for enough small  $u$  quark mass. This work and our preliminary lattice simulation reported here for  $\pi K$  scattering lengths will encourage the researchers to study the  $\kappa$  resonance. We are beginning a series of lattice investigations on the  $\kappa$  resonance parameters with isospin representation of  $(I, I_z) = (1/2, 1/2)$ , and the preliminary results are already reported in Refs. [33, 54].

## Acknowledgments

This work is supported in part by Fundamental Research Funds for the Central Universities (2010SCU23002) and the Startup Grant from the Institute of Nuclear Science and Technology of Sichuan University. The author thanks Carleton DeTar for kindly providing us the MILC gauge configurations used for this work and the fitting software to analyze the lattice data. We are indebted to the MILC collaboration for using the Asqtad lattice ensemble and MILC codes. We are grateful to Hou Qing for his comprehensive supports. The computations for this work were carried out at AMAX, CENTOS and HP workstations in the Institute of Nuclear Science and Technology, Sichuan University.

## Appendix A: The calculation method of zeta function

In this appendix we briefly discuss one method for numerical evaluation of zeta function  $\mathcal{Z}_{00}(s; q^2)$  in the center-of-mass system for any value of  $q^2$ . Here we follow the original derivations and notations in Ref. [26].

The definition of zeta function  $\mathcal{Z}_{00}(s; q^2)$  in Eq. (13) is

$$\sqrt{4\pi} \cdot \mathcal{Z}_{00}(s; q^2) = \sum_{\mathbf{n} \in \mathbb{Z}^3} \frac{1}{(n^2 - q^2)^s}. \quad (\text{A1})$$

The zeta function  $\mathcal{Z}_{00}(s; q^2)$  takes a finite value for  $\text{Re } s > 3/2$ , and  $\mathcal{Z}_{00}(1; q^2)$ , is defined by the analytic continuation from the region  $\text{Re } s > 3/2$ .

First we consider the case of  $q^2 > 0$ , and we separate the summation in  $\mathcal{Z}_{00}(s; q^2)$  into two parts as

$$\sum_{\mathbf{n} \in \mathbb{Z}^3} \frac{1}{(n^2 - q^2)^s} = \sum_{n^2 < q^2} \frac{1}{(n^2 - q^2)^s} + \sum_{n^2 > q^2} \frac{1}{(n^2 - q^2)^s}, \quad (\text{A2})$$

The second term can be written in an integral form,

$$\begin{aligned} \sum_{n^2 > q^2} \frac{1}{(n^2 - q^2)^s} &= \frac{1}{\Gamma(s)} \sum_{n^2 > q^2} \left[ \int_0^1 dt t^{s-1} e^{-t(n^2 - q^2)} + \int_1^\infty dt t^{s-1} e^{-t(n^2 - q^2)} \right] \\ &= \frac{1}{\Gamma(s)} \int_0^1 dt t^{s-1} e^{q^2 t} \sum_{\mathbf{n} \in \mathbb{Z}^3} e^{-n^2 t} - \sum_{n^2 < q^2} \frac{1}{(n^2 - q^2)^s} + \sum_{\mathbf{n} \in \mathbb{Z}^3} \frac{e^{-(n^2 - q^2)}}{(n^2 - q^2)^s}. \end{aligned} \quad (\text{A3})$$

The second term neatly cancels out the first term in Eq. (A2). Next we rewrite the first term in Eq. (A3) by the Poisson's resummation formula as,

$$\begin{aligned} \frac{1}{\Gamma(s)} \int_0^1 dt t^{s-1} e^{tq^2} \sum_{\mathbf{n} \in \mathbb{Z}^3} e^{-n^2 t} &= \\ \frac{1}{\Gamma(s)} \int_0^1 dt t^{s-1} e^{tq^2} \left(\frac{\pi}{t}\right)^{3/2} \sum_{\mathbf{n} \in \mathbb{Z}^3} e^{-\pi^2 n^2 / t}. \end{aligned} \quad (\text{A4})$$

The divergence at  $s = 1$  comes from the  $\mathbf{n} = \mathbf{0}$  part of the integrand on the right-hand side, therefore we divide

the integrand into a divergent part ( $\mathbf{n} = \mathbf{0}$ ) and a finite part ( $\mathbf{n} \neq \mathbf{0}$ ). The divergent part can be evaluated for  $\text{Re } s > 3/2$  as

$$\int_0^1 dt t^{s-1} e^{q^2 t} \left(\frac{\pi}{t}\right)^{3/2} = \sum_{l=0}^{\infty} \frac{\pi^{3/2}}{s + l - 3/2} \frac{q^{2l}}{l!}. \quad (\text{A5})$$

The right hand side of this equation takes a finite value at  $s = 1$ .

After gathering all terms we obtain the representation of the zeta function in the center-of-mass system at  $s = 1$ ,

$$\sqrt{4\pi} \cdot \mathcal{Z}_{00}(s; q^2) = \sum_{\mathbf{n} \in \mathbb{Z}^3} \frac{e^{-(n^2 - q^2)}}{n^2 - q^2} + \sum_{l=0}^{\infty} \frac{\pi^{3/2}}{l - 1/2} \frac{q^{2l}}{l!} + \int_0^1 dt e^{q^2 t} \left(\frac{\pi}{t}\right)^{3/2} \sum'_{\mathbf{n} \in \mathbb{Z}^3} e^{-\pi^2 n^2 / t}, \quad (\text{A6})$$

where  $\sum'_{\mathbf{n} \in \mathbb{Z}^3}$  stands for a summation without  $\mathbf{n} = \mathbf{0}$ .

For the case of  $q^2 \leq 0$ , it is not necessary for us to separate the summation in  $\mathcal{Z}_{00}(s; q^2)$ , and it can be also written in an integral form,

$$\begin{aligned} \sum_{\mathbf{n} \in \mathbb{Z}^3} \frac{1}{(n^2 - q^2)^s} &= \\ \frac{1}{\Gamma(s)} \int_0^1 dt t^{s-1} e^{q^2 t} \sum_{\mathbf{n} \in \mathbb{Z}^3} e^{-n^2 t} + \sum_{\mathbf{n} \in \mathbb{Z}^3} \frac{e^{-(n^2 - q^2)}}{(n^2 - q^2)^s}. \end{aligned} \quad (\text{A7})$$

Following the same procedures, we arrive at the same expression in Eq. (A6). Hence, Eq. (A6) can be applied for both cases.

We also note that, for negative  $q^2$ , an exponentially convergent expression of the zeta function  $\mathcal{Z}_{00}(s; q^2)$  has been derived in Ref. [55]. We numerically compared this representation of the zeta functions with that of above described representation, and found agreement. Therefore, we use Eq. (A6) in this work.

- [1] M.J. Matison *et al.*, Phys. Rev. D, **9**, 1872 (1974).
- [2] N.O. Johannesson and J.L. Petersen, Nucl. Phys. **B68**, 397, 1973.
- [3] A. Karabouraris and G. Shaw, J. Phys. G, **6**, 583, 1980.
- [4] <http://dirac.web.cern.ch/DIRAC/future.html>.
- [5] J. M. Flynn and J. Nieves, Phys. Rev. D **75**, 074024 (2007).
- [6] V. Bernard, N. Kaiser, U. G. Meissner, Nucl. Phys. **B357**, 129 (1991).
- [7] V. Bernard, N. Kaiser, U. G. Meissner, Phys. Rev. D **43**, 2757 (1991).
- [8] B. Kubis and U. G. Meissner, Phys. Lett. B **529**, 69 (2002).
- [9] P. Buettiker, S. Descotes-Genon, and B. Moussallam, hep-ph/0310283, 2003.

- [10] C. Miao, X. Du, G. Meng, C. Liu, Phys. Lett. B **595**, 400 (2004).
- [11] S. R. Beane, P. F. Bedaque, T. C. Luu, K. Orginos, E. Pallante, A. Parreno and M. J. Savage, Phys. Rev. D **74**, 114503 (2006).
- [12] J. Nagata, S. Muroya, A. Nakamura, Phys. Rev. C **80**, 045203 (2009).
- [13] K. Sasaki, N. Ishizuka, T. Yamazaki and M. Oka, Prog. Theor. Phys. Suppl. **186**, 187 (2010).
- [14] K. Orginos and D. Toussaint [MILC Collaboration], Phys. Rev. D **59**, 014501 (1998).
- [15] K. Orginos, D. Toussaint and R. L. Sugar [MILC Collaboration], Phys. Rev. D **60**, 054503 (1999).
- [16] C. Bernard *et al.*, Phys. Rev. D **83**, 034503 (2011).
- [17] A. Bazavov *et al.*, Rev. Mod. Phys. **82**, 1349 (2010).

- [18] Y. Kuramashi, M. Fukugita, H. Mino, M. Okawa and A. Ukawa, Phys. Rev. Lett. **71**, 2387 (1993).
- [19] M. Luscher, Nucl. Phys. **B354**, 531 (1991).
- [20] M. Luscher, U. Wolff, Nucl. Phys. **B339**, 222 (1990).
- [21] L. Lellouch and M. Luscher, Commun. Math. Phys. **219**, 31 (2001).
- [22] M. Fukugita, Y. Kuramashi, H. Mino, M. Okawa, A. Ukawa, Phys. Rev. Lett. **73**, 2176 (1994).
- [23] M. Fukugita, Y. Kuramashi, M. Okawa, H. Mino and A. Ukawa, Phys. Rev. D **52**, 3003 (1995).
- [24] S. R. Sharpe, R. Gupta and G. W. Kilcup, Nucl. Phys. **B383**, 309 (1992).
- [25] R. Gupta, G. Guralnik, G. W. Kilcup, S. R. Sharpe, Phys. Rev. D **43**, 2003 (1991).
- [26] T. Yamazaki *et al.*, Phys. Rev. D **70**, 074513 (2004)
- [27] A. Mihály, H. R. Fiebig, H. Markum and K. Rabitsch, Phys. Rev. D **55**, 3077 (1997).
- [28] A. Mihály, “Studies of Meson-Meson Interactions within Lattice QCD”, PhD thesis, Lajos Kossuth University, Debrecen, 1998.
- [29] C. Aubin *et al.*, Phys. Rev. D **70**, 094505 (2004).
- [30] C. W. Bernard *et al.*, Phys. Rev. D **64**, 054506 (2001).
- [31] Z. Fu, Chin. Phys. C **37**, 1079 (2011).
- [32] Z. Fu, arXiv:1111.1835 [hep-lat] (Accepted for publication in Chin. Phys. C).
- [33] Z. Fu, JHEP **01**, 017 (2012) [arXiv:1110.5975 [hep-lat]].
- [34] C. Aubin and C. Bernard, Phys. Rev. D **68**, 034014 (2003).
- [35] C. Bernard, C. E. DeTar, Z. Fu and S. Prelovsek, Phys. Rev. D **76**, 094504 (2007).
- [36] C. W. Bernard, C. E. DeTar, Z. Fu and S. Prelovsek, PoS **LAT2006**, 173 (2006).
- [37] D. B. Kaplan, Phys. Lett. B **288**, 342 (1992).
- [38] Y. Shamir, Nucl. Phys. **B406**, 90 (1993).
- [39] Y. Shamir, Phys. Rev. D **59**, 054506 (1999).
- [40] A. Hasenfratz and F. Knechtli, Phys. Rev. D **64**, 034504 (2001).
- [41] T. A. DeGrand, A. Hasenfratz and T. G. Kovacs, Phys. Rev. D **67**, 054501 (2003).
- [42] T. A. DeGrand [MILC Collaboration], Phys. Rev. D **69**, 014504 (2004).
- [43] S. Durr, C. Hoelbling and U. Wenger, Phys. Rev. D **70**, 094502 (2004).
- [44] D. B. Renner *et al.* [LHP Collaboration], Nucl. Phys. Proc. Suppl. **140**, 255 (2005).
- [45] R. G. Edwards *et al.* [LHPC Collaboration], PoS **LAT2005**, 056 (2006).
- [46] S. Aoki *et al.* [CP-PACS Collaboration], Phys. Rev. D **76**, 094506 (2007).
- [47] Z. Fu, Chin. Phys. Lett. **28**, 081202 (2011).
- [48] C. Aubin *et al.*, Phys. Rev. D **70**, 114501 (2004).
- [49] Z. Fu, Commun. Theor. Phys. **57**, 78 (2012).
- [50] J. W. Chen, D. O’Connell and A. Walker-Loud, Phys. Rev. D **75**, 054501 (2007).
- [51] J. Gasser and H. Leutwyler, Nucl. Phys. **B250**, 465 (1985).
- [52] K. Nakamura *et al.* (Particle Data Group), J. Phys. G **37**, 075021 (2010).
- [53] S. Aoki *et al.*, Phys. Rev. D **79**, 034503 (2009).
- [54] Z. Fu, Phys. Rev. D **85**, 014506 (2012).
- [55] E. Elizalde, Commun. Math. Phys. **198**, 83 (1998).